frontiers | Frontiers in Chemistry

TYPE Original Research
PUBLISHED 19 October 2022
DOI 10.3389/fchem.2022.1025030

OPEN ACCESS

EDITED BY
Shahid Zaman,
Southern University of Science and Technology, China

REVIEWED BY
Sikandar Khan,
King Fahd University of Petroleum and Minerals, Saudi Arabia
Malik Ashtar,
Jiangsu University, China
Muhammad Usman,
King Fahd University of Petroleum and Minerals, Saudi Arabia

*CORRESPONDENCE
Xiu-Jian Wang,
wang1_xj@aliyun.com
Taj Malook Khan,
tajmalook83@swmu.edu.cn

†These authors have contributed equally to this work

SPECIALTY SECTION
This article was submitted to Electrochemistry, a section of the journal Frontiers in Chemistry

RECEIVED 22 August 2022
ACCEPTED 26 September 2022
PUBLISHED 19 October 2022

CITATION
Khan A, Gul NS, Luo M, Wu J, Khan SZ, Manan A, Wang X-J and Khan TM (2022), Fabrication of a lead-free ternary ceramic system for high energy storage applications in dielectric capacitors. *Front. Chem.* 10:1025030. doi: 10.3389/fchem.2022.1025030

Fabrication of a lead-free ternary ceramic system for high energy storage applications in dielectric capacitors

Azam Khan[1†], Noor Shad Gul[2,3†], Mao Luo[2,3], Jianbo Wu[2,3], Shahan Zeb Khan[4], Abdul Manan[5], Xiu-Jian Wang[1*] and Taj Malook Khan[2,3*]

[1]School of Chemistry and Pharmacy, Guangxi Normal University, Guilin, China, [2]Drug Discovery Research Center, Southwest Medical University, Luzhou, China, [3]Department of Pharmacology, Laboratory for Cardiovascular Pharmacology, School of Pharmacy, Southwest Medical University, Luzhou, China, [4]Department of Chemistry, University of Science and Technology, Bannu, Pakistan, [5]Advanced Materials Research Laboratory, Department of Physics, University of Science and Technology Bannu, Bannu, Pakistan

The importance of electroceramics is well-recognized in applications of high energy storage density of dielectric ceramic capacitors. Despite the excellent properties, lead-free alternatives are highly desirous owing to their environmental friendliness for energy storage applications. Herein, we provide a facile synthesis of lead-free ferroelectric ceramic perovskite material demonstrating enhanced energy storage density. The ceramic material with a series of composition (1-z) ($0.94Na_{0.5}Bi_{0.5}TiO_3$-$0.06BaTiO_3$)-z$Nd_{0.33}NbO_3$, denoted as NBT-BT-zNN, where, z = 0.00, 0.02, 0.04, 0.06, and 0.08 are synthesized by the conventional solid-state mix oxide route. Microphases, microstructures, and energy storage characteristics of the as-synthesized ceramic compositions were determined by advanced ceramic techniques. Powder X-ray diffraction analysis reveals pure single perovskite phases for z = 0 and 0.02, and secondary phases of $Bi_2Ti_2O_7$ appeared for z = 0.04 and 0.08. Furthermore, scanning electron microscopy analysis demonstrates packed-shaped microstructures with a reduced grain size for these ceramic compositions. The coercive field (E_c) and remnant polarization (P_r) deduced from polarization vs. electric field hysteresis loops determined using an LCR meter demonstrate decreasing trends with the increasing z content for each composition. Consequently, the maximum energy storage density of 3.2 J/cm^3, the recoverable stored energy of 2.01 J/cm^3, and the efficiency of 62.5% were obtained for the z content of 2 mol% at an applied electric field of 250 kV/cm. This work demonstrates important development in ceramic perovskite for high power energy storage density and efficiency in dielectric capacitors in high-temperature environments. The aforementioned method makes it feasible to modify a binary ceramic composition into a ternary system with highly enhanced energy storage characteristics by incorporating rare earth metals with transition metal oxides in appropriate proportions.

KEYWORDS

perovskite, recoverable energy, pulsed power, dielectric capacitors, temperature

Introduction

The world leaders have signed the Paris Agreement on climate change to fix global warming <1.5°C by reducing the emission of greenhouse gases by the end of 2030 and reaching zero levels by 2050 (Vicedo-Cabrera et al., 2018). In recent years, the emission of CO_2 has increased immensely in the upper atmosphere due to the burning of fossil fuels for transportation, domestic uses, and industrial developments. Hence, this tremendous amount of CO_2 has seriously impaired the Earth's environment due to the greenhouse effect that caused global warming, climate change, and acidification of oceanic water (Letcher, 2020; Chen et al., 2022). The feasible solution for both these issues of global warming and climate change is to substitute fossil fuel energy sources with renewable energy sources such as sunlight, tides, waves, and wind power as clean and free of greenhouse gases (Panwar et al., 2011; Lima et al., 2020). The energy produced from these inexhaustible energy resources needs energy storage materials and devices to store it for future use without disturbing the Earth's environment (Timmons et al., 2014; Krishan & Suhag, 2019). In this regard, dielectric materials with high energy storage density can be used to miniaturize the component employed in most electronic devices (Kyerematen et al., 2017; Liu et al., 2019). Currently, most energy storage technologies are based on batteries, fuel cells, supercapacitors, and dielectric capacitors (Winter & Brodd, 2004; Kim et al., 2015; Wu et al., 2019). Compared to batteries and fuel cells, capacitors are highly cost-effective, stable thermally, and robust, working with high power density. Numerous dielectric capacitors are based on polymers and ceramics with high output power, fast charge–discharge rate, and long working life in high-temperature environments (Fan et al., 2018; Palneedi et al., 2018; Zhou et al., 2018). Dielectric ceramic-based capacitors are superior to polymer-based dielectrics owing to their stable energy potential and working at a broader temperature range. However, dielectric ceramics have a drawback of low energy storing density compared to dielectric polymers because of their low dielectric breakdown strength (DBS), which reduces their range of applications (Zeb & Milne, 2015; Li Q et al., 2018; Zaman, et al., 2021a). Thus, developing new dielectric ceramic systems with high energy storage density is more valuable for miniaturization, integration, and lightweight energy storage devices under high-temperature conditions (Jiang et al., 2021; Yang et al., 2019; Zaman, et al., 2022a).

Typically, ceramic materials applied for dielectric capacitors have linear dielectric, ferroelectric, anti-ferroelectric, and relaxor ferroelectric characteristics (Zheng et al., 2021; Zhou et al., 2020). The recoverable energy density (W_{rec}) is deduced from the energy storage ability of dielectric substances. The recoverable and storage energy densities are evaluated mathematically in Eqs 1,2 (Wang et al., 2019).

$$W_s = \int_0^{P_{max}} EdP \tag{1}$$

$$W_{rec} = \int_{P_r}^{P_{max}} EdP \tag{2}$$

The efficiency can be determined from Eq. 3 as follows:

$$\eta = W_{res}/W_s \times 100\,\% \tag{3}$$

The aforementioned equations show that maximum polarization (P_{max}), high permittivity, large DBS, and low remnant polarization (P_r) are crucial for dielectric ceramics to achieve maximum storage power density and high efficiency. In this regard, an enormous amount of research has been carried out for lead-containing dielectric ceramics owing to their high energy storage characteristics such as (Pb, La)ZrO_3 (PLZ), Pb(Zr, Sn, Ti)O_3 (PZST), and (Pb, La) (Zr, Ti)O_3 (PLZT) (Parui & Krupanidhi, 2008; Jia et al., 2018). However, lead-consistent ceramics are toxic and have an environmental impact; therefore, lead-free ceramic compositions with high energy storage characteristics must be fabricated. In this regard, a lead-free ceramic composition $Na_{0.5}Bi_{0.5}TiO_3$ (NBT) has received greater attention since it has a large maximum polarization (P_{max}~40 μC/cm^2) and high Curie temperature (T_c~320°C); however, it has large remnant polarization (P_r) and high coercive field (E_c) as well which make it unsuitable for energy storage applications (Li K et al., 2018; Ranjan, 2020). Therefore, massive research has been carried out in fabricating binary or ternary solid solutions of NBT by modifying it with $Bi_{0.5}$ $K_{0.5}TiO_3$ (KBT), $K_{0.5}Na_{0.5}NbO_3$ (KNN), and BaTiO3 (BT) for enhancing its energy storage competencies (Quan et al., 2014; Wong et al., 2015; Zhao et al., 2016; Zaman, et al., 2022b). Hence, Takenaka et al. (1991) prepared $NBT_{1-x}BT$ (BNBT) by adding $BaTiO_3$ and studied its morphotropic phase boundary (MPB), developed for x ~ 6–7 mol% for the assurance of large ferroelectric and piezoelectric characteristics in comparison with lead-consistent ceramics. In the same way, Li et al. (2016) fabricated a ceramic composition of 0.94Bi0.5Na0.5TiO3-0.06BaTiO3-0.03$CaZrO_3$ *via* adding $CaZrO_3$ has displayed an energy storage density of W_s ~ 0.70 J/cm^3. Likewise, J. Wang and Chen, (2014) prepared a ceramic composition of $0.92Na_{0.47}Bi_{0.47}Ba_{0.06}TiO_3-0.08KNbO_3$ by adding $KNbO_3$ which resulted in W_s ~ 0.89 J/cm^3. In the same way, Li et al. (2019) fabricated a modified ceramic composition of 0.85 $[(Na_{0.5}Bi_{0.5})_{0.94}Ba_{0.06}]TiO_3-0.15BaSnO_3$ by adding $BaSnO_3$, which demonstrated an enhanced W_s ~ 1.20 J/cm^3 and efficiency of 86.7%. In this connection, J. Ding et al. (2014) also achieved W_s ~ 0.90 J/cm^3 for 0.89Bi0.5Na0.5TiO3-0.06BaTiO3-0.05K0.5Na0.5NbO3. These results demonstrate that the appropriate cation addition of alkali, alkaline earth, and rare

earth metals at either A or B sites of ABO_3 structure of $(Na_{0.5}Bi_{0.5})_{0.94}Ba_{0.06}TiO_3$) has reduced its E_c, which resulted in enhanced energy storage characteristics of this composition. The addition of $Nd_{0.33}$ NbO_3 into the $(Na_{0.5}Bi_{0.5})_{0.94}Ba_{0.06}TiO_3$) system suppressed its ferroelectric loops with the decreasing remnant polarization, which resulted in increased energy storage competencies in this ceramic composition (Jain et al., 2021; Huang et al., 2022).

The present work focuses on modifying the ceramic composition of $0.94(Na_{0.5}Bi_{0.5})TiO_3$-$0.06BaTiO_3$ by introducing $Nd_{0.33}$ NbO_3 to investigate its effects on the coercive field and remnant polarization. The influences of $Nd_{0.33}$ NbO_3 addition on the aforementioned composition have been studied in energy storage density, recoverable energy, and efficiency as a function of z content under high-temperature conditions.

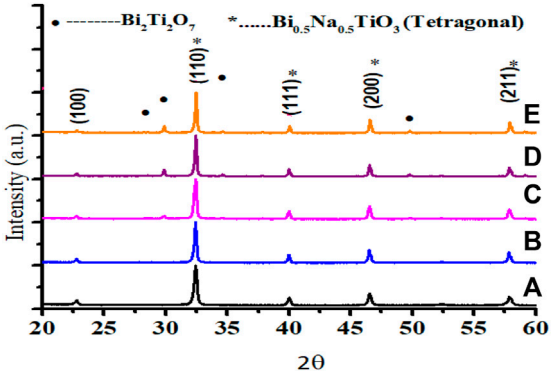

FIGURE 1
X-ray diffraction (XRD) patterns for (NBT-BT-zNN) **(A)** z = 0.00, **(B)** z = 0.02, **(C)** z = 0.04, **(D)** z = 0.06, and **(E)** z = 0.08.

Experimental protocols

Several methods are used for the fabrication of lead-free electroceramic compositions, such as mechanochemical synthesis, sol–gel method, and current-assisted sintering method; however, in the bulk of electroceramic fabrication, the most common preparation method is solid-state mix oxide synthesis, typically from metal oxide–carbonate mixtures, and sintering. We employed a conventional solid-state mix oxide method to synthesize (NBT-BT-zNN), (z = 0.00, 0.02, 0.04, 0.06, 0.08) ceramic compositions, using the reagents: $BaCO_3$ (99.9%), Bi_2O_3 (99%), TiO_2 (99.8%), Na_2CO_3 (99.8%), Nb_2O_5 (99%), and Nd_2O_3 (99.9%). These starting raw materials in powder forms were heated at 100°C for two days before weighing their stoichiometric amounts to remove the trapped water moisture from bodies. The reagents were weighed stoichiometrically and then ball-milled with ethanol in plastic containers using ZrO_2 grinding balls for 24 h, resulting in the formation of slurries, which were then dried at 95°C temperature. The milled powder of each composition was heated for 2 h at 850°C and then re-ball-milled for 12 h and dried to get fine powders. A few drops of liquid polyvinyl alcohol (PVA) as a binder were mixed with the dried samples and ground for 10 min. After completing this process, each sample was pressed to make a pellet of 1 mm height at a force of 150 MPa in a steel die of 12 mm diameter. These pellets were heated for 2 h at 600°C to remove PVA content and finally sintered at 1,050°C, 1,150°C, and 1,175°C for 2 h. The green body pellets of each composition were sintered at different temperatures, such as 1,050, 1,150, and 1,175°C, for 2 h to get the optimum density of each composition. We measure the density of each composition at the aforementioned temperatures using the Archimedes principle. The results showed that the density was higher at 1,150°C for each ceramic composition, and each composition's properties were determined for the optimally dense sintered ceramics at 1,150°C for 2 h.

At the maximum density, a pellet of each sample was crushed and converted to powders. The phase analysis was carried out for the sintered samples using a powder X-ray diffraction technique. Using an X-ray diffractometer, the data were recorded at a scan rate of 0.02°/min at 2θ from 10–80°. For the microstructural study, a maximally dense pellet of each sample was smoothly polished and then thermally etched, followed by a gold coating to avoid the charging effect during the electron beam interaction. The microstructure of each sample was checked using a scanning electron microscope.

Furthermore, both the surfaces of a thick pellet of 0.65 mm thickness of each ceramic composition sintered at 1,150°C were highly polished, followed by a silver coating, and heated at 800°C for 2 h. The dielectric constant and tangent loss in each sample on 400, 550, 800, and 1 MHz vs. temperature were noted with a scan rate of 3°C/min using the LCR meter (Agilent E4980 A). The thickness of maximum dense samples was minimized up to 0.15 μm, then coated with silver films, and heated at 800°C for 2 h. Polarization vs. electric field (P-E) loops at breakdown voltage were taken at 10 Hz using a ferroelectric test method.

Results and discussion

Phases and microstructures interpretation

Figure 1 shows typical PXRD patterns of ceramic compositions (1-z) (NBT-BT-zNN), (z = 0.00, 0.02, 0.04, 0.06, 0.08) recorded at room temperature with 2θ = 20–60°. The observed peaks labelled as "*" in XRD patterns were matched with PDF (070–4760), a single perovskite phase for z = 0.00 and z = 0.02, demonstrating complete diffusion of $Nd_{0.33}NbO_3$ into (NBT-BT) lattices and resulting in a slight expansion due to which (111) and (200) peaks have moved to a lower angle with the increasing content of $Nd_{0.33}NbO_3$. At the same time, a few low-intensity peaks labelled as "•" also appeared for z ≥ 0.04. These peaks matched with PDF (089–4732) and labelled as "•"

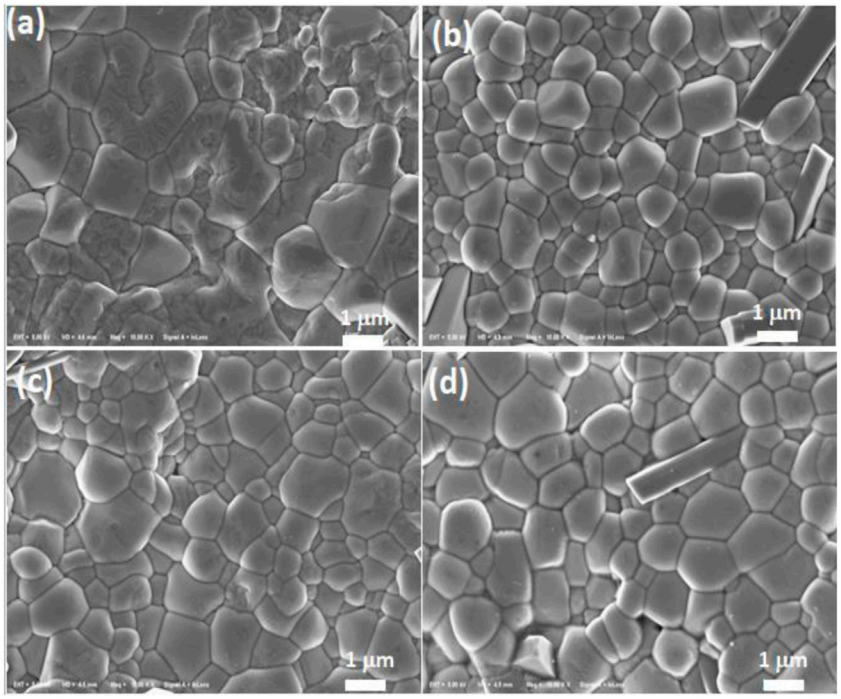

FIGURE 2
Scanning electron micrographs from thermally etched surfaces for (NBT-BT-zNN) **(A)** z = 0.00, **(B)** z = 0.02, **(C)** z = 0.04, and **(D)** z = 0.08.

exhibited the secondary phase ($Bi_2Ti_2O_7$). The developments of the secondary phase indicate the solid solubility limit of $Nd_{0.33}NbO_3$ in the $0.94Bi_{0.5}Na_{0.5}TiO_3$-$0.06BaTiO_3$ system of about 2 mol%. Previous studies also demonstrated the appearance of this $Bi_2Ti_2O_7$ secondary phase in $Bi_{0.5}Na_{0.5}TiO_3$-$BaTiO_3$-based ceramics (Ding et al., 2022; Lu et al., 2011; Ni et al., 2012; Wang et al., 2022). This secondary phase $Bi_2Ti_2O_7$ appeared due to the vaporization of Bi and Na at elevated temperatures (Xu et al., 2015). Furthermore, the value of $Bi_2Ti_2O_7$ has increased with the increasing z content to 8 mol% in this current formulation.

Figure 2 displays the scanning electron micrographs of (NBT-BT-zNN), z = 0.00, 0.02, 0.04, and 0.08). There are clear grain boundaries observed for all the compositions with dense microstructures. Grain sizes are decreased with increasing z contents of $z \leq 0.06$ and then slightly increased to the z content of 0.08. Several factors, including the liquid phase, dopants, and pore/voids, could affect the grain growth (Xu et al., 2017; H. Yang et al., 2017; Z. Yang et al., 2016). The increasing amount and ionic radii of Nb^{5+} (0.64 Å) against Ti^{4+} (0.60 Å) may also result in lower ionic mobility upon sintering and hence hinder the diffusion of ions that resulted in the slowdown of grain growth (Zaman et al., 2021). The regular distribution of grains is highly effective in increasing density and enhancing the DBS of dielectric ceramics (Begum et al., 2021; Fernandez-Benavides et al., 2018; Li et al., 2021). Some plates like elongated grains is observed in the microstructures reported in the previous literature (Wood et al., 1999).

Dielectric characteristics

Figure 3 depicts the temperature-dependent variation of the relative permittivity (ε_r) and tan δ (loss of the energy rate, also known as the dissipation factor) for (NBT-BT-zNN), (z = 0.00, 0.02, 0.04, and 0.08) ceramics measured at 400 kHz, 550 kHz, 850 kHz, and 1 MHz with a temperature of 25–500°C. Two peaks were observed in each ε_r curve with temperature variation. The peak at a lower temperature is called the depolarization temperature (T_d), and the other peak (T_m) shows the maxima of the dielectric constant at high temperature, called the Curie temperature. These two anomalies are also observed in BNT ceramics (Trolliard & Dorcet, 2008; Jo et al., 2011; Butnoi et al., 2018). The anti-ferroelectric-to-paraelectric phase transformation is observed across the Curie temperature (T_m) (Pan et al., 2019). A frequency dispersion and phase transition peak of the ferroelectric-to-paraelectric phase of (NBT-BT-zNN) ceramics demonstrated distorted long-range ordering of the ferroelectric phase to develop relaxor nature. Likewise, T_d has shifted toward high temperature upon the variation of frequency from 450 kHz to 1 MHz, indicating an increase in

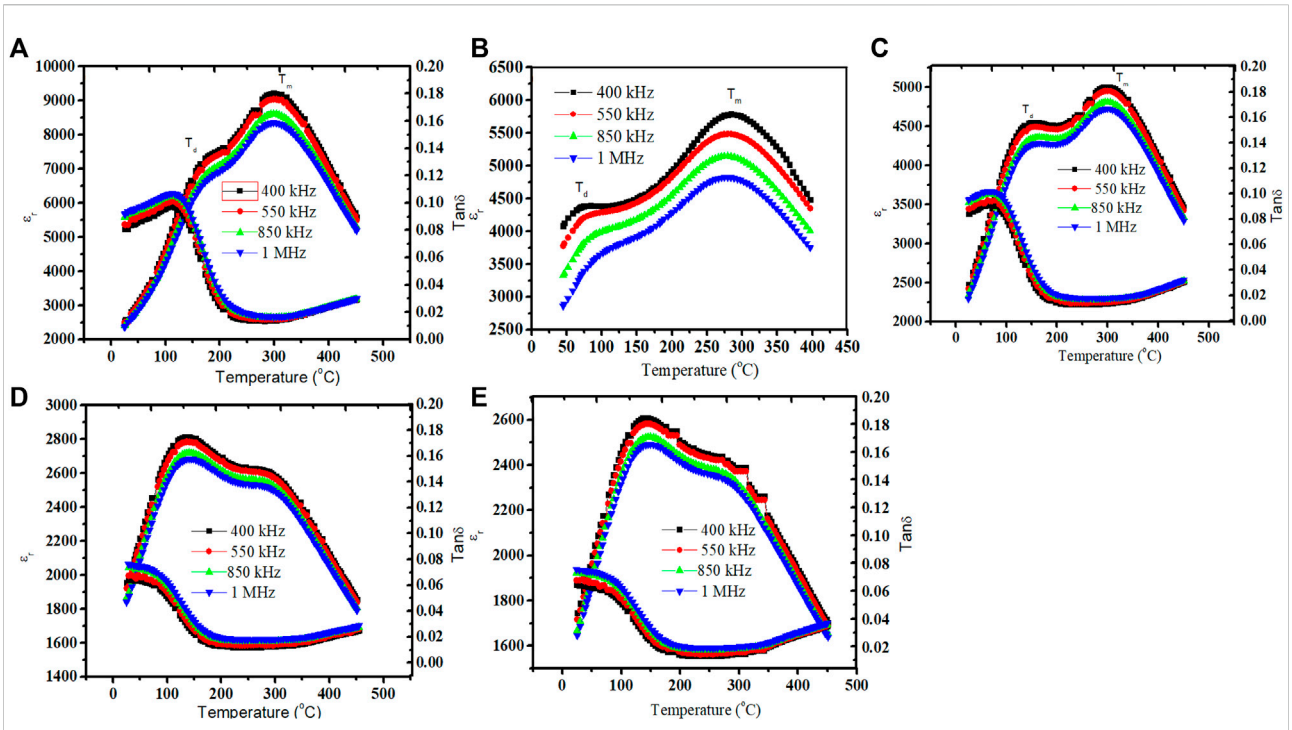

FIGURE 3
Changes in ε_r and tan δ measured at different frequencies for (NBT-BT-zNN) **(A)** z = 0.00, **(B)** z = 0.02, **(C)** z = 0.04, **(D)** z = 0.06, and **(E)** z = 0.08 with changes in temperature.

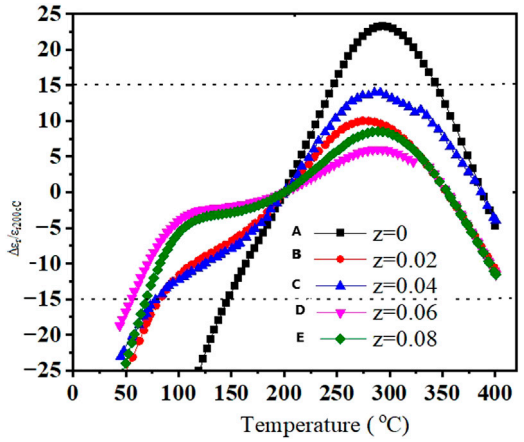

FIGURE 4
Changes in $\Delta\varepsilon_r/\varepsilon_{r200}$°C for (NBT-BT-zNN) **(A)** z = 0.00, **(B)** z = 0.02, **(C)** z = 0.04, **(D)** z = 0.06, and **(E)** z = 0.08 ceramics with temperature at 1 MHz.

the relaxor behavior. Furthermore, T_d observed >150°C at 1 kHz but gradually moved to a lower temperature (<75°C) upon increasing the z content. The broadening of the ε_r versus T curve between T_d and T_m shows an improvement in the stability of energy storage characteristics with temperature. Furthermore, adding the z content has decreased T_m and ε_m of these ceramics (Dittmer et al., 2012; Pradhan et al., 2018; Jin, Li, & Zhang, 2020).

The stable nature of the ceramic's dielectric constant with temperature is another important parameter. There are changes observed in permittivity (± 15%) in the temperature range of 44–400°C for (z = 0.00, 0.02, 0.04, and 0.08) ceramics, measured at 1 MHz using Eq. 4, as shown in Figure 4.

$$\Delta\varepsilon_r/\varepsilon_r200°C, \tag{4}$$

where $\Delta\varepsilon_r = \varepsilon_rT\text{-}\varepsilon_r200°C$. $\Delta\varepsilon_r/\varepsilon_{r200}$°C for a sample of z = 0.02 displayed good thermal stability in the temperature range of 83–420°C. Similarly, z = 0.6 also displayed thermal stability in the temperature range of 55–430°C.

Ferroelectricity and energy storage characteristics

The polarization vs. electric field (P–E) hysteresis loops with a frequency of 10 Hz were recorded at 25°C for (NBT-BT-zNN), (z = 0.00, 0.02, 0.04, and 0.08) ceramics, as shown in Figure 5. The observed P-E loop became slim with the increased z content, showing enhancement in the ferroelectric nature of the $0.94Na_{0.5}Bi_{0.5}TiO_3\text{-}0.06BaTiO_3$ ceramic system. The increase in

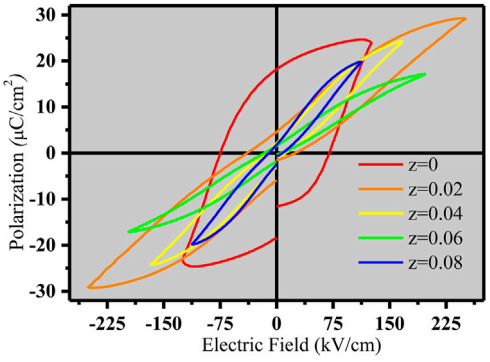

FIGURE 5
Polarization versus electric field (P-E) hysteresis loops of (1-z) (NBT-BT-zNN) ceramics.

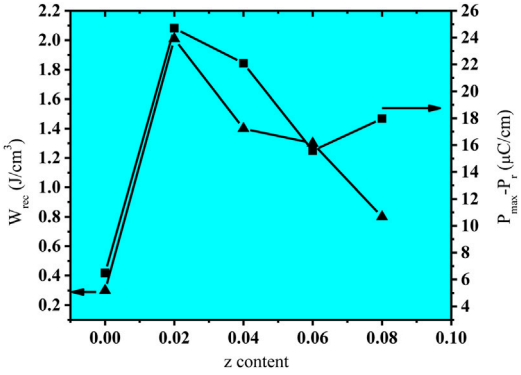

FIGURE 7
Changes in W_{rec} and P_{max}-P_r for (NBT-BT-zNN) ceramics with the z content.

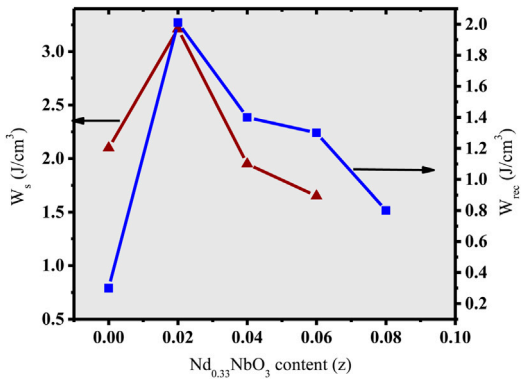

FIGURE 6
Changes in W_s and W_{rec} of (NBT-BT-zNN) ceramics with the z content.

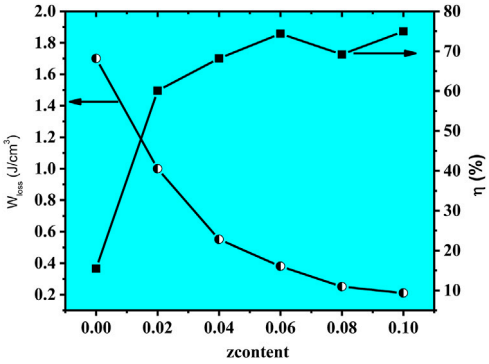

FIGURE 8
Changes in W_{loss} and η of (NBT-BT-zNN) ceramics with the z content.

the z content has decreased the remnant polarization (P_r), suggesting the Nb^{5+} substitution for Ti^{4+} at the B-site and Nd^{3+} for (Ba^{2+}/Bi^{3+}/Na^{1+}) at the A-site disrupting the long-range ordering of domains and converting it to the polar nano-regions (PNRs) (Mayamae et al., 2016; Hu et al., 2018). The sizes of PNRs are small as compared to the ferroelectric micro-domain. The PNRs can easily be aligned back and forth by the applied electric field, which causes a decrease in the P_r value (Wen et al., 2018).

Figure 5 shows a double double-like P-E hysteresis loop for the (NBT-BT-zNN) ceramic system with a good anti-ferroelectric behavior for z = 0.02, which is very important for energy storage applications. This anti-ferroelectric behavior is also observed in the NBT-BT-La system (P. Fan et al., 2021; Liu et al., 2013). The doping of the z content decreased Pr, resulting in depolarization at room temperature. Keeping of the high-electric field has generated electric field-induced polarization that caused a decrease in P_r and an increase in the W_{rec} value. Thus, a decreased P_r value has increased the W_{rec} value for the (NBT-BT-zNN) ceramic system at 250 kV/cm for the z content of 2 mol%.

The recoverable energy density (W_{rec}) and energy storage density (W_s) for the (NBT-BT-zNN) ceramic system is determined at the maximum applied electric field, as shown in Figure 6. The energy storage and recoverable energy density initially increased with the x content from 0 to 0.02 and then decreased with a further increase in the x content to 0.1. Both are related to the large and high breakdown strength. Furthermore, it is also reported that W_{rec} energy density strongly depends on P_{max}-P_r. The large value of P_{mx}-P_r results into high W_{rec}. Therefore, the high value of W_{rec} in the present study for x = 0.02 is also because of its large P_{max}-P_r value compared to other x values, as shown in Figure 7. The large value of P_{max}-P_r is related to its high breakdown strength and the lower remnant polarization. The increased breakdown electric field (E_b) and large $\Delta P = P_{max}$-P_r value ensure a large value of W_{rec} for x = 0.02. Hence, W_s~3.2 J/cm^3 along

with W_{rec}~2.01 J/cm^3 and efficiency of η~62.5% were obtained for z = 0.02 at 250 kV/cm, as demonstrated in Figure 8. The large W_{rec} value is related to the anti-ferroelectric response induced in this parent formulation (0.94($Na_{0.5}Bi_{0.5}$)TiO_3-0.06$BaTiO_3$) due to $Nd_{0.33}NbO_3$ doping up to 2 mol%.

Conclusion

Capacitors based on relaxor dielectrics are promising candidates for pulsed power applications as they have high energy storage capabilities, high output power, fast charging–discharging rate, and good electric breakdown strength performances under high-temperature conditions. These (NBT-BT-zNN), (z = 0.00, 0.02, 0.04, 0.08) ceramic compositions have been processed by the conventional solid-state mix oxide route, and their dielectric properties, phases, microstructure, and storage energy density were investigated. For z ≤ 0.02, a single perovskite phase was formed, while for z = 0.04, a secondary phase $Bi_2Ti_2O_7$ also developed. The highly dense microstructural feature appeared for each ceramic. The high energy storage density W_s ~ 3.2 J/cm^3 and recoverable energy W_{rec} ~ 2.01 J/cm^3 with an efficiency of 62.5% were achieved for the composition with the z content of 2 mol% at an electric field of 250 kV/cm, which is a worthy opening in the developments of high-temperature-sustainable ceramic materials for dielectric capacitors.

Data availability statement

The raw data supporting the conclusion of this article will be made available by the authors, without undue reservation.

Author contributions

AK: Conceptualization, Methodology, Software, Validation. ML and JW are responsible for resources. AM: Data curation, Writing-Draft preparation. SZK: Reviewing and Editing. X-JW: Visualization, Investigation. TMK and NSG: Supervision.

Funding

This work was supported by the Drug Discovery Research Center, Southwest Medical University, Luzhou, China, under Grant No. 42-00040176, which was awarded to TMK.

Conflict of interest

The authors declare that the research was conducted in the absence of any commercial or financial relationships that could be construed as a potential conflict of interest.

Publisher's note

All claims expressed in this article are solely those of the authors and do not necessarily represent those of their affiliated organizations, or those of the publisher, the editors, and the reviewers. Any product that may be evaluated in this article, or claim that may be made by its manufacturer, is not guaranteed or endorsed by the publisher.

References

Begum, S., Yuhana, N. Y., Saleh, N. M., Kamarudin, N. H. N., and Sulong, A. B. (2021). Review of chitosan composite as a heavy metal adsorbent: Material preparation and properties. *Carbohydr. Polym.* 259, 117613. doi:10.1016/j.carbpol.2021.117613

Butnoi, P., Manotham, S., Jaita, P., Randorn, C., and Rujijanagul, G. (2018). High thermal stability of energy storage density and large strain improvement of lead-free Bi0. 5 (Na0. 40K0. 10) TiO_3 piezoelectric ceramics doped with La and Zr. *J. Eur. Ceram. Soc.* 38 (11), 3822–3832. doi:10.1016/j.jeurceramsoc.2018.04.024

Chen, S., Zhang, Z., Jiang, W., Zhang, S., Zhu, J., Wang, L., et al. (2022). Engineering water molecules activation center on multisite electrocatalysts for enhanced CO2 methanation. *J. Am. Chem. Soc.* 144 (28), 12807–12815. doi:10.1021/jacs.2c03875

Ding, J., Liu, Y., Lu, Y., Qian, H., Gao, H., Chen, H., et al. (2014). Enhanced energy-storage properties of 0.89 Bi0. 5Na0. 5TiO_3–0.06 BaTiO3–0.05 K0. 5Na0. 5NbO_3 lead-free anti-ferroelectric ceramics by two-step sintering method. *Mat. Lett.* 114, 107–110. doi:10.1016/j.matlet.2013.09.103

Ding, Y., Que, W., He, J., Bai, W., Zheng, P., Li, P., et al. (2022). Realizing high-performance capacitive energy storage in lead-free relaxor ferroelectrics via synergistic effect design. *J. Eur. Ceram. Soc.* 42 (1), 129–139. doi:10.1016/j.jeurceramsoc.2021.09.051

Dittmer, R., Anton, E. M., Jo, W., Simons, H., Daniels, J. E., Hoffman, M., et al. (2012). A high-temperature-capacitor dielectric based on K 0.5 Na 0.5 NbO 3-modified Bi 1/2 Na 1/2 TiO 3–Bi 1/2 K 1/2 TiO 3. *J. Am. Ceram. Soc.* 95 (11), 3519–3524. doi:10.1111/j.1551-2916.2012.05321.x

Fan, B., Liu, F., Yang, G., Li, H., Zhang, G., Jiang, S., et al. (2018). Dielectric materials for high-temperature capacitors. *IET Nanodielectrics* 1 (1), 32–40. doi:10.1049/iet-nde.2018.0002

Fan, P., Liu, K., Ma, W., Tan, H., Zhang, Q., Zhang, L., et al. (2021). Progress and perspective of high strain NBT-based lead-free piezoceramics and multilayer actuators. *J. Materiomics* 7 (3), 508–544. doi:10.1016/j.jmat.2020.11.009

Fernandez-Benavides, D. A., Gutierrez-Perez, A. I., Benitez-Castro, A. M., Ayala-Ayala, M. T., Moreno-Murguia, B., and Muñoz-Saldaña, J. (2018). Comparative study of ferroelectric and piezoelectric properties of BNT-BKT-BT ceramics near the phase transition zone. *Materials* 11 (3), 361. doi:10.3390/ma11030361

Hu, B., Fan, H., Ning, L., Wen, Y., and Wang, C. (2018). High energy storage performance of [(Bi0.5Na0.5)0.94Ba0.06]0.97La0.03Ti1-(Al0.5Nb0.5) O3 ceramics with enhanced dielectric breakdown strength. *Ceram. Int.* 44 (13), 15160–15166. doi:10.1016/j.ceramint.2018.05.154

Huang, Q., Si, F., and Tang, B. (2022). The effect of rare-earth oxides on the energy storage performances in BaTiO3 based ceramics. *Ceram. Int.* 48 (12), 17359–17368. doi:10.1016/j.ceramint.2022.02.299

Jain, A., Wang, Y., and Guo, H. (2021). Emergence of relaxor behavior along with enhancement in energy storage performance in light rare-earth doped Ba0. 90Ca0. 10Ti0. 90Zr0. 10O3 ceramics. *Ceram. Int.* 47 (8), 10590–10602. doi:10.1016/j.ceramint.2020.12.171

Jia, W., Hou, Y., Zheng, M., Xu, Y., Zhu, M., Yang, K., et al. (2018). Advances in lead-free high-temperature dielectric materials for ceramic capacitor application. *IET Nanodielectrics* 1 (1), 3–16. doi:10.1049/iet-nde.2017.0003

Jiang, J., Meng, X., Li, L., Zhang, J., Guo, S., Wang, J., et al. (2021). Enhanced energy storage properties of lead-free NaNbO3-based ceramics via A/B-site substitution. *Chem. Eng. J.* 422, 130130. doi:10.1016/j.cej.2021.130130

Jin, L., Li, F., and Zhang, S. (2020). "Decoding the fingerprint of ferroelectric loops: Comprehension of the material properties and structures," in *Progress in J. Adv. Dielectr.* (Singapore: World Scientific), 21–104. doi:10.1142/9789811210433_0002

Jo, W., Schaab, S., Sapper, E., Schmitt, L. A., Kleebe, H.-J., Bell, A. J., et al. (2011). On the phase identity and its thermal evolution of lead free (Bi1/2Na1/2) TiO3-6 mol% BaTiO3. *J. Appl. Phys.* 110 (7), 074106. doi:10.1063/1.3645054

Kim, B. K., Sy, S., Yu, A., and Zhang, J. (2015). Electrochemical supercapacitors for energy storage and conversion. *J Handb. clean energy syst* 2015, 1–25. doi:10.1002/9781118991978.hces112

Krishan, O., and Suhag, S. (2019). An updated review of energy storage systems: Classification and applications in distributed generation power systems incorporating renewable energy resources. *Int. J. Energy Res.* 43 (12), 6171–6210. doi:10.1002/er.4285

Kyerematen, N. A., Brousse, T., and Pech, D. (2017). Micro supercapacitors as miniaturized energy-storage components for on-chip electronics. *Nat. Nanotechnol.* 12 (1), 7–15. doi:10.1038/nnano.2016.196

Li, K., Luo, L., Zhang, Y., Li, W., and Hou, Y. (2018). Tunable luminescence contrast in photochromic ceramics (1–x) Na0. 5Bi0. 5TiO3–x Na0. 5K0. 5NbO3: 0.002 Er by an electric field poling. *ACS Appl. Mat. Interfaces* 10 (48), 41525–41534. doi:10.1021/acsami.8b15784

Li, Q., Yao, F.-Z., Liu, Y., Zhang, G., Wang, H., and Wang, Q. (2018). High-temperature dielectric materials for electrical energy storage. *Annu. Rev. Mat. Res.* 48, 219–243. doi:10.1146/annurev-matsci-070317-124435

Letcher, T. M. (2020). "Introduction with a focus on atmospheric carbon dioxide and climate change," in *Future energy* (Amsterdam, Netherlands: Elsevier), 3–17. doi:10.1016/B978-0-08-102886-5.00001-3

Li, Q., Li, M., Wang, C., Zhang, M., and Fan, H. (2019). Enhanced temperature stable dielectric properties and energy-storage density of BaSnO3-modified (Bi0. 5Na0. 5) 0.94 Ba0. 06TiO3 lead-free ceramics. *Ceram. Int.* 45 (16), 19822–19828. doi:10.1016/j.ceramint.2019.06.237

Li, Q., Wang, J., Ma, Y., Ma, L., Dong, G., and Fan, H. (2016). Enhanced energy-storage performance and dielectric characterization of 0.94 Bi0. 5Na0. 5TiO3–0.06 BaTiO3 modified by CaZrO3. *J. Alloys Compd.* 663, 701–707. doi:10.1016/j.jallcom.2015.12.194

Li, Y., Liu, Y., Tang, M., Lv, J., Chen, F., Li, Q., et al. (2021). Energy storage performance of BaTiO3-based relaxor ferroelectric ceramics prepared through a two-step process. *Chem. Eng. J.* 419, 129673. doi:10.1016/j.cej.2021.129673

Lima, M., Mendes, L., Mothé, G., Linhares, F., de Castro, M., Da Silva, M., et al. (2020). Renewable energy in reducing greenhouse gas emissions: Reaching the goals of the Paris agreement in Brazil. *Environ. Dev.* 33, 100504. doi:10.1016/j.envdev.2020.100504

Liu, L.-Y., Wang, R.-Z., Zhu, M.-K., and Hou, Y.-D. (2013). Site occupation of doping La^{3+} cations and phase transition in Na0. 5Bi0. 5TiO3-BaTiO3 solid solution. *Chin. Phys. B* 22 (3), 036401. doi:10.1088/1674-1056/22/3/036401

Liu, S., Shen, B., Hao, H., and Zhai, J. (2019). Glass-ceramic dielectric materials with high energy density and ultra-fast discharge speed for high power energy storage applications. *J. Mat. Chem. C Mat.* 7 (48), 15118–15135. doi:10.1039/C9TC05253D

Lu, W., Wang, Y., Fan, G., Wang, X., and Liang, F. (2011). The structural and electric properties of Li-and K-substituted Bi0. 5Na0. 5TiO3 ferroelectric ceramics. *J. Alloys Compd.* 509 (6), 2738–2744. doi:10.1016/j.jallcom.2010.10.041

Mayamae, J., Sukkha, U., Niemchareon, S., Muanghlua, R., and Vittayakorn, N. J. F. (2016). Dielectric, ferroelectric and piezoelectric properties of the lead-free 0.9 BaTiO3-(0.1-x) Bi0. 5Na0. 5TiO3-x Bi (Mg0. 5Ti0. 5) O3 solid solution. *Ferroelectrics* 490 (1), 23–35. doi:10.1080/00150193.2015.1070656

Ni, F., Luo, L., Pan, X., Li, W., and Zhu, J.(2012). Effects of A-site vacancy on the electrical properties in lead-free non-stoichiometric ceramics Bi0. 5+ x (Na0. 82K0. 18) 0.5– 3xTiO3 and Bi0. 5+ y (Na0. 82K0. 18) 0.5 TiO3. *J. Alloys Compd.* 541, 150–156. doi:10.1016/j.jallcom.2012.06.129

Palneedi, H., Peddigari, M., Hwang, G. T., Jeong, D. Y., and Ryu, J. (2018). High-performance dielectric ceramic films for energy storage capacitors: Progress and outlook. *Adv. Funct. Mat.* 28 (42), 1803665. doi:10.1002/adfm.201803665

Pan, Z., Hu, D., Zhang, Y., Liu, J., Shen, B., and Zhai, J. (2019). Achieving high discharge energy density and efficiency with NBT-based ceramics for application in capacitors. *J. Mat. Chem. C Mat.* 7 (14), 4072–4078. doi:10.1039/C9TC00087A

Panwar, N., Kaushik, S., and Kothari, S. (2011). Role of renewable energy sources in environmental protection: A review. *Renew. Sustain. Energy Rev.* 15 (3), 1513–1524. doi:10.1016/j.rser.2010.11.037

Parui, J., and Krupanidhi, S. (2008). Enhancement of charge and energy storage in sol-gel derived pure and La-modified Pb Zr O 3 thin films. *Appl. Phys. Lett.* 92 (19), 192901. doi:10.1063/1.2928230

Pradhan, L. K., Pandey, R., Kumar, S., Supriya, S., and Kar, M. (2018). Octahedral distortion due to oxygen vacancy reduction in La3+ modified BNT-BTO solid solutions near morphotropic phase boundary. *J. Phys. D. Appl. Phys.* 51 (37), 375301. doi:10.1088/1361-6463/aad50d

Quan, N. D., Huu Bac, L., Thiet, D. V., Hung, V. N., and Dung, D. D. (2014). Current development in lead-FreeBi0.5(Na, K)0.5TiO3-based piezoelectric MaterialsCurrent development in lead-free-based piezoelectric materials. *Adv. Mater. Sci. Eng.* 2014, 1–13. doi:10.1155/2014/365391

Ranjan, R. (2020). Na1/2Bi1/2TiO3-based lead-free piezoceramics: A review of structure-property correlation. *Curr. Sci.* 118 (10), 1507. doi:10.18520/cs/v118/i10/1507-1519

Takenaka, T., Maruyama, K.-I. M. K.-I., and Sakata, K. S. K. (1991). Bi1/2Na1/2) TiO3-BaTiO3 system for lead-free piezoelectric ceramics. *Jpn. J. Appl. Phys.* 30, 2236. doi:10.1143/JJAP.30.2236

Timmons, D., Harris, J. M., and Roach, B. (2014). The economics of renewable energy. *Int. J. Glob. Environ.* 52, 1–52.

Trolliard, G., Dorcet, V., and Boullay, P. (2008). Reinvestigation of phase transitions in $Na_{0.5}Bi_{0.5}TiO_3$ by TEM. Part I: First order rhombohedral to orthorhombic phase transition. *Chem. Mat.* 20 (15), 5061–5073. doi:10.1021/cm8004634

Vicedo-Cabrera, A. M., Guo, Y., Sera, F., Huber, V., Schleussner, C.-F., Mitchell, D., et al. (2018). Temperature-related mortality impacts under and beyond Paris Agreement climate change scenarios. *Clim. Change* 150 (3), 391–402. doi:10.1007/s10584-018-2274-3

Wang, C., Ma, T., Zhang, Y., and Huang, H. (2022). Versatile titanates: Classification, property, preparation, and sustainable energy catalysis. *Adv. Funct. Mat.* 32 (5), 2108350. doi:10.1002/adfm.202108350

Wang, H., Liu, Y., Yang, T., and Zhang, S. (2019). Ultrahigh energy-storage density in anti-ferroelectric ceramics with field-induced multiphase transitions. *Adv. Funct. Mat.* 29 (7), 1807321. doi:10.1002/adfm.201807321

Wang, J., and Chen, C. (2014). Chitosan-based biosorbents: Modification and application for biosorption of heavy metals and radionuclides. *Bioresour. Technol.* 160, 129–141. doi:10.1016/j.biortech.2013.12.110

Wen, Y., Zhang, J., Xu, Q., Wu, X.-T., and Zhu, Q.-L. (2018). Pore surface engineering of metal-organic frameworks for heterogeneous catalysis. *Coord. Chem. Rev.* 376, 248–276. doi:10.1016/j.ccr.2018.08.012

Winter, M., and Brodd, R. (2004). What are batteries, fuel cells, and supercapacitors? *Chem. Rev.* 104 (10), 4245–4270. doi:10.1021/cr020730k

Wong, J. Y. Y. (2015). Synthesis and characterization of lead-free perovskite solid solutions Science: Department of Chemistry. Burnaby, Canada: Simon fraser university. Thesis.

Wood, C. A., Zhao, H., and Cheng, Y. B. (1999). Microstructural development of calcium alpha-SiAlON ceramics with elongated grains. *J. Am. Ceram. Soc.* 82 (2), 421–428. doi:10.1111/j.1551-2916.1999.tb20079.x

Wu, Y., Fan, Y., Liu, N., Peng, P., Zhou, M., Yan, S., et al. (2019). Enhanced energy storage properties in sodium bismuth titanate-based ceramics for dielectric capacitor applications. *J. Mat. Chem. C Mat.* 7 (21), 6222–6230. doi:10.1039/C9TC01239G

Xu, Q., Li, T., Hao, H., Zhang, S., Wang, Z., Cao, M., et al. (2015). Enhanced energy storage properties of NaNbO3 modified Bi0. 5Na0. 5TiO3-based ceramics. *J. Eur. Ceram. Soc.* 35 (2), 545–553. doi:10.1016/j.jeurceramsoc.2014.09.003

Xu, Q., Xie, J., He, Z., Zhang, L., Cao, M., Huang, X., et al. (2017). Energy-storage properties of Bi0.5Na0.5TiO3-BaTiO3-KNbO3 ceramics fabricated by wet-chemical method. *J. Eur. Ceram. Soc.* 37 (1), 99–106. doi:10.1016/j.jeurceramsoc.2016.07.011

Yang, H., Yan, F., Lin, Y., Wang, T., Wang, F., Wang, Y., et al. (2017). Lead-free BaTiO3-Bi0. 5Na0. 5TiO3-Na0. 73Bi0. 09NbO3 relaxor ferroelectric ceramics for high energy storage. *J. Eur. Ceram. Soc.* 37 (10), 3303–3311. doi:10.1016/j.jeurceramsoc.2017.03.071

Yang, L., Kong, X., Li, F., Hao, H., Cheng, Z., Liu, H., et al. (2019). Perovskite lead-free dielectrics for energy storage applications. *Prog. Mat. Sci.* 102, 72–108. doi:10.1016/j.pmatsci.2018.12.005

Yang, Z., Du, H., Qu, S., Hou, Y., Ma, H., Wang, J., et al. (2016). Significantly enhanced recoverable energy storage density in potassium–sodium niobate-based lead free ceramics. *J. Mat. Chem. A Mat.* 4 (36), 13778–13785. doi:10.1039/C6TA04107H

Zaman, A., Uddin, S., Mehboob, N., Ali, A., Ahmad, A., and Bashir, K. J. F. (2021). Effect of Zr4+ on the structural and microwave dielectric properties of CaTiO3 ceramics. *Ferroelectrics* 577 (1), 143–152. doi:10.1080/00150193.2021.1916357

Zaman, S., Su, Y. Q., Dong, C. L., Qi, R., Huang, L., Qin, Y., et al. (2022a). Scalable molten salt synthesis of platinum alloys planted in metal-nitrogen-graphene for efficient oxygen reduction. *Angew. Chem. Int. Ed. Engl.* 61 (6), 202115835–202115843. doi:10.1002/anie.202115835

Zaman, S., Tian, X., Su, Y.-Q., Cai, W., Yan, Y., Qi, R., et al. (2021a). Direct integration of ultralow-platinum alloy into nanocarbon architectures for efficient oxygen reduction in fuel cells. *Sci. Bull. (Beijing).* 66 (21), 2207–2216. doi:10.1016/j.scib.2021.07.001

Zaman, S., Wang, M., Liu, H., Sun, F., Yu, Y., Shui, J., et al. (2022b). Carbon-based catalyst supports for oxygen reduction in proton-exchange membrane fuel cells. *Trends Chem*. 4, p886-p906. doi:10.1016/j.trechm.2022.1007.1007

Zeb, A., and Milne, S. (2015). High temperature dielectric ceramics: A review of temperature-stable high-permittivity perovskites. *J. Mat. Sci. Mat. Electron.* 26 (12), 9243–9255. doi:10.1007/s10854-015-3707-7

Zhao, J., Cao, M., Wang, Z., Xu, Q., Zhang, L., Yao, Z., et al. (2016). Enhancement of energy-storage properties of K0. 5Na0. 5NbO3 modified Na0. 5Bi0. 5TiO3–K0. 5Bi0. 5TiO3 lead-free ceramics. *J. Mat. Sci. Mat. Electron.* 27 (1), 466–473. doi:10.1007/s10854-015-3775-8

Zheng, L., Sun, P., Zheng, P., Bai, W., Li, L., Wen, F., et al. (2021). Significantly tailored energy-storage performances in Bi 0.5 Na 0.5 TiO 3–SrTiO 3-based relaxor ferroelectric ceramics by introducing bismuth layer-structured relaxor BaBi2Nb2O9 for capacitor application. *J. Mat. Chem. C Mat.* 9 (15), 5234–5243. doi:10.1039/D1TC00437A

Zhou, M., Liang, R., Zhou, Z., and Dong, X. (2020). Developing a novel high-performance NaNbO3-based lead-free dielectric capacitor for energy storage applications. *Sustain. Energy Fuels* 4 (3), 1225–1233. doi:10.1039/c9se00836e

Zhou, Y., Li, Q., Dang, B., Yang, Y., Shao, T., Li, H., et al. (2018). A scalable, high-throughput, and environmentally benign approach to polymer dielectrics exhibiting significantly improved capacitive performance at high temperatures. *Adv. Mat.* 30 (49), 1805672. doi:10.1002/adma.201805672